Nuclear Materials and Energy 38 (2024) 101577

Contents lists available at ScienceDirect

Nuclear Materials and Energy

journal homepage: www.elsevier.com/locate/nme

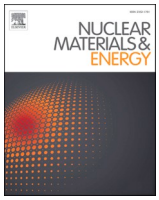

Initial experiments to regenerate the surface of plasma-facing components by wire-based laser metal deposition

Jannik Tweer [a,b,c,*], Robin Day [b], Thomas Derra [b], Daniel Dorow-Gerspach [a], Thorsten Loewenhoff [a], Marius Wirtz [a], Christian Linsmeier [a], Thomas Bergs [b,d], Ghaleb Natour [e,f]

[a] Forschungszentrum Jülich GmbH, Institut für Energie- und Klimaforschung - Plasmaphysik, 52425 Jülich, Germany
[b] Fraunhofer Institute for Production Technology IPT, 52074 Aachen, Germany
[c] RWTH Aachen University, Fakultät für Maschinenwesen, 52056 Aachen, Germany
[d] Laboratory for Machine Tools and Production Engineering (WZL) of RWTH Aachen University, 52074 Aachen, Germany
[e] Forschungszentrum Jülich GmbH, Zentralinstitut für Engineering, Elektronik und Analytik, 52425 Jülich, Germany
[f] RWTH Aachen University, Lehrstuhl und Institut für Schweißtechnik und Fügetechnik, 52062 Aachen, Germany

ARTICLE INFO

Keywords:
Nuclear fusion
Additive Manufacturing (AM)
Wire-based Laser Metal Deposition (LMD-w)
Surface regeneration
Tungsten (W)

ABSTRACT

Plasma-facing components (PFC) in nuclear fusion reactors are exposed to demanding conditions during operation. The combination of thermal loads, plasma exposure as well as neutron induced damage and activation limits the number of materials suitable for this application. Due to its properties, tungsten (W) is foreseen as plasma-facing material (PFM) for the future DEMOnstration power plant. It is considered suitable due to its exceptionally high melting point, excellent thermal conductivity, low tritium retention and low erosion resistance during plasma exposure. But even tungsten armored PFCs have a limited lifetime due to, among other factors, surface erosion and the resulting thickness reduction of the armor material.

In-situ local deposition of tungsten by means of additive manufacturing (AM) could counteract surface erosion and thus increase the service life span of PFCs. After evaluation of the potential AM processes qualified for this task, the wire-based laser metal deposition (LMD-w) process was selected as the most suitable process. First trials were conducted to examine if it is possible to reliably deposit tungsten onto tungsten substrate using the LMD-w process. In these first studies, single welding beads were generated, and in later experiments, entire layers were created from several welding beads which are arranged next to each other. To ensure reproducibility of the results, the substrate temperature was kept constant. Further experiments aimed at the elimination or minimization of problems such as oxidation, occurrence of balling defects, porosity, cracking, surface waviness and insufficient connection to the substrate. To increase the welding bead quality, the input parameters like laser power, deposition velocity, wire feed rate, inert gas flow, as well as the wire position were optimized. Furthermore, stacking of several layers, as well as the remelting of an already created layer, were carried out and investigated. This study represents the first steps in testing the feasibility of an in-situ surface regeneration concept for PFCs.

1. Introduction

The plasma-facing components (PFC) in future fusion reactors like the DEMOnstration power plant will be confronted with a variety of challenges. Tungsten is the most suitable candidate for the armor material of PFCs due to its comparatively low erosion rate, good thermal conductivity of approximately 160 W m^{-1} K^{-1}, superior melting point (T_{melt} = 3695 K), low tritium retention and resilient nature[1–3]. For the future DEMOnstration power plant, an armor material erosion of 0.3 mm per full power year is expected with tungsten as plasma-facing material [4]. The properties of tungsten are required since the PFM has to withstand stationary heat loads in the MW/m^2 range as well as transient loads mainly in form of edge localized modes (ELMs) in the GW/m^2 range [5]. Vertical displacement events (VDEs) and plasma disruptions known as off normal events place even higher thermal loads and particle fluxes on the PFM [6,7]. These transient heat loads can lead to the melting of even tungsten and subsequently increase the erosion rate. Due to unpreventable erosion losses, the tungsten armor thickness

* Corresponding author at: Forschungszentrum Jülich GmbH, Institut für Energie- und Klimaforschung - Plasmaphysik, 52425 Jülich, Germany.
E-mail address: j.tweer@fz-juelich.de (J. Tweer).

https://doi.org/10.1016/j.nme.2023.101577
Received 13 October 2023; Received in revised form 20 December 2023; Accepted 27 December 2023
Available online 28 December 2023

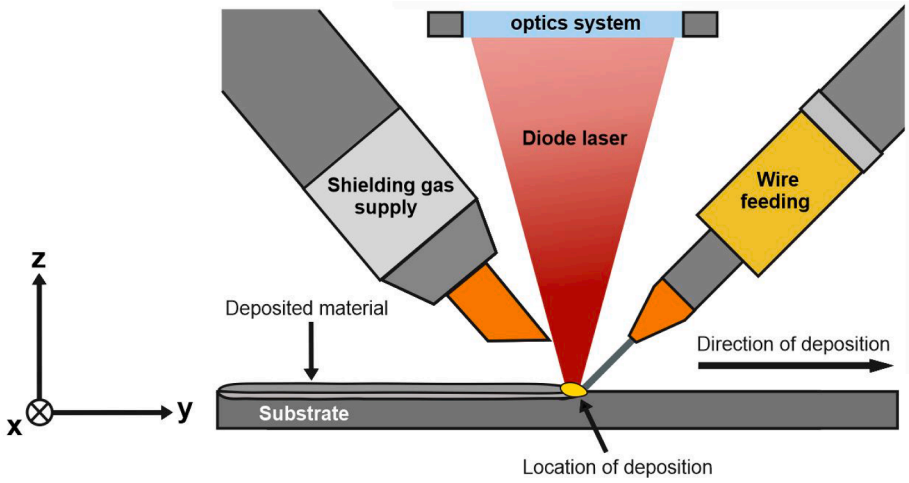

Fig. 1. Schematic representation of material deposition by LMD-w processing.

in future fusion reactors is designed large enough to not fall below the minimum thickness even after heavy erosion losses [8]. However, the shorter the distance from the surface of the PFM to the coolant, the lower the surface temperature of the PFC. This usually means lower thermal stresses and hence a longer lifetime. Thus, small armor layer thicknesses are desirable. The surface regeneration concept presented here offers an opportunity to use a thin PFM armor right from the start. Even if just small areas of the PFC reach the end of their service life, for example at the strike line in the divertor section, the entire PFC must still be replaced. With the possibility of local in situ repair this replacement could be avoided, respectively the service life could be extended.

Whether this kind of surface regeneration of PFCs is possible at all has yet to be clarified. First, it has to be shown whether it is technically feasible to deposit tungsten on tungsten with sufficient quality, accuracy, and deposition rate. The broad field of additive manufacturing processes offers a range of options for this purpose. Since powder-bed based processes, such as laser powder bed fusion (LPBF) [9,10] or electron beam melting process [11], are not suitable for in situ repairs, these processes are excluded from the selection despite their proven material quality. On the other hand directed energy deposition (DED) processes are particularly effective for the local application of metal [12]. However, there are several limiting factors that need to be considered. For example, uncontrolled deposition or distribution within the reactor is not allowed to occur, since this may endanger plasma operation, or have other negative effects like increased erosion. Thus the occurrence of loose material residues should be avoided at all costs, because especially high z materials like tungsten cool down the plasma significantly by Bremsstrahlung and radiation losses [13]. Due to the contamination by incompletely or not at all melted powder during the process, powder-based DED processes are excluded. Another limiting factor is the constrained space within the vessel that is available for in situ repair. Furthermore, the repair process should be able to work in vacuum as this reduces possible contamination and it is not clear whether the repair would be performed under atmospheric or vacuum conditions. Unlike conventional powder based laser metal deposition (LMD) or the wire-arc additive manufacturing (WAAM) process, wire-based laser metal deposition (LMD-w) does not produce welding spatters or powder residues. Sufficient accuracy is required for repairing the PFC and LMD-w is much more accurate than the WAAM process. Consequently, the LMD-w process was selected as the most suitable process. Furthermore, the LMD process has the advantage that the laser source can be positioned outside the vessel and the light can be guided easily via fiber optic cables to the designated process location. It is envisioned to repair the PFC using an LMD-w processing head, such as the already existing LMD-W-20-L model, attached to a robotic arm to operate inside the vessel [14].

Although there is already a limited amount of literature on the processing of pure tungsten by DED in the form of powder based LMD [15,16] or WAAM available [17,18] no studies have yet been conducted on the processing of tungsten by LMD-w. In the wire-based laser metal deposition a laser beam gets focused on a substrate and creates a melt pool. Then a wire is fed directly into the melt pool or the laser focal point of the laser. This way material is applied locally and connected to the substrate. In Fig. 1 a schematic representation of material deposition by LMD-w processing is illustrated. Compared to other DED processes, LMD-w meets all the requirements to operate clean inside future fusion reactors. Compared to electron beam welding, laser processes require less space and no vacuum, as the laser source could be located outside the vessel and could be routed to the operating location by fiber optic cables. The LMD-w process can provide deposition rates of up to 1 kg/h with a material efficiency of nearly 100 % [19]. This study represents the proof-of-principle to process pure tungsten by LMD-w. Parameter studies were performed starting from single beads over whole layers, up to stacked layers. Furthermore, to improve the quality of the deposit, the usage of remelting was investigated.

2. Experimental

Commercially available pure tungsten wire from Osram Licht AG with a diameter of 1 mm was utilized as base material for deposition in the following experiments. Rolled pure tungsten plates were chosen as the substrate material to represent the armor of plasma facing components. These plates were cut by electrical discharge machining (EDM) from larger tungsten blanks and subsequently etched to remove contaminations and Cu remains from the EDM.

A Laserline GmbH (model LDF 5000-40) diode laser delivers power of up to 5 kW. This continuous wave laser operates in the wavelength range from 910 nm to 1,030 nm. The light is directed to the optics via glass fibers. A water-cooled optic system from Laserline GmbH directs the light onto a focal point. The optical system creates a Gaussian beam profile with a spot diameter of 2 mm. The optimal focal distance measures 139 mm from the optics to the substrate. The wire is guided by a wire feeding system by Abicor Binzel. A computerized numerical control (CNC) 3-axis system allows the machine table to move in the x- and y-direction as well as the LMD-w system to move in the z-direction. The machine is controlled by means of a Rexroth system console.

To find suitable process parameters for the processing of tungsten with the LMD-w process, various parametric studies were conducted. Compared to the materials usually deposited using the LMD-w process, a much higher energy input is required to process tungsten due to its high

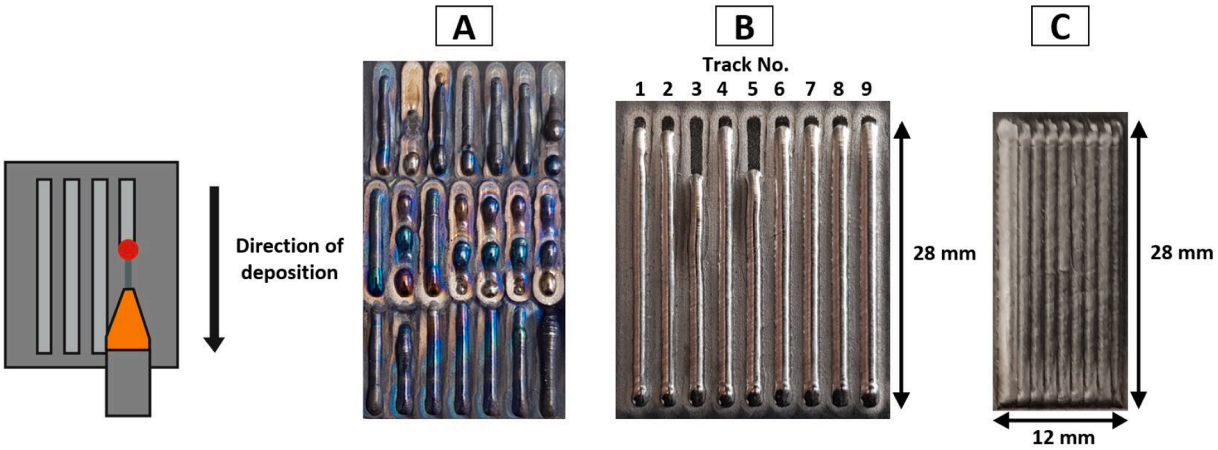

Fig. 2. Images of LMD-w welding beads and a layer. (A) showing preliminary investigation samples, which contain various defects. (B) is displaying 9 of the overall 45 welding beads generated for the parametric study to optimize the creation of single welding beads. (C) is an LMD-w layer covering an area of 28 × 12 mm^2, which was deposited with the process parameters listed in Table 3.

Table 1
Overview of the various parameters used in the experiments for single welding beads, layers, and the remelting of layers.

Experiment	Symbol	Welding beads	Layers	Layer remelting	Unit
Energy per unit area	E_n	191–458	191–477	477–955	J mm^{-2}
Laser power	P	4–4.8	4–5	5	kW
Deposition velocity	v_t	400–800	400–800	200–400	mm min^{-1}
Wire fed velocity	v_w	600–1200	500–2000	–	mm min^{-1}
Deposition length	L	28	14–28	14	mm
Hatch distance	h_d	–	1.12–1.51	1.51	mm

melting point. This high energy input results in strong heating of the substrate plate, which leads to increasing substrate temperatures the longer the process lasts. To reduce this temperature drift and obtain reproducible results, the substrate plate was kept at a constant temperature of 19 °C by means of a water-cooled copper plate. This also had the effect of avoiding the formation of undesirable oxidation traces, which posed a problem in preliminary studies. The substrate plate was pressed against the cooling structure using two screwed down copper plates.

The LMD-w process is influenced by several factors, such as laser power, deposition velocity, wire fed velocity, wire position, wire feeding angle, substrate temperature, ambient temperature, inert gas flow rate, deposition direction, etc. The results of these mentioned preliminary tests are shown in Fig. 2 (A) and revealed that it is by no means trivial to deposit tungsten at all using the LMD-w process with this particular setup. Due to the large number of adjustable influencing variables a systematic cause-and-effect study of each parameter would require an unreasonably large quantity of tests. Therefore, the range of reasonable parameters was determined by calculations and in the preliminary tests. More elaborated parametric studies were subsequently carried out in these reasonable ranges in order to further optimize the process. To derive the influence of the individual parameters with the highest impact, only the laser power, tool velocity, wire fed velocity, hatch and wire position were varied in the experiments discussed here. The other influencing parameters were set to reasonable values that were determined empirically.

Preliminary studies showed that the dragging process (i.e., front feeding process) had a slightly higher stability with tungsten than the piercing process (i.e., rear feeding process). Furthermore, the process performed well with a wire feeding angle of 45 degrees. Therefore, the dragging process with a wire feeding angle of 45 degrees was used for all the experiments conducted in this study. The experiments took place in a normal atmosphere and different gas flow rates of argon, delivered through the gas nozzle shown in Fig. 1, were tested to shield the deposited tungsten from possible contamination. A gas flow rate of 15 l min^{-1} showed the best results and was set as standard for the following experiments. The waiting time between the individual welding beads was set to 10 s for all experiments in order to give the substrate plate sufficient time to cool down. The intent was to ensure that the substrate plate had the same initial temperature before the start of each welding bead. Table 1 provides an overview of the most relevant process parameters used for the tests performed. To compare the amount of energy introduced, an energy per unit area is calculated for the individual parameter sets using the following equation [20]:

$$E_n = \frac{4P}{\pi d_s v_t}\left[Jmm^{-2}\right] \tag{1}$$

Where P is the laser power, d_s the diameter of the laser focal spot and v_t the deposition velocity. The minimum intensity required by a laser beam to melt a material can be approximated by the following equation [21,22]:

$$I_{th_{min}} = \frac{k(T)\Delta T}{A(\lambda,T)d_s J_{max}}\left[Wmm^{-2}\right] \tag{2}$$

Where $k(T)$ is the temperature dependent thermal conductivity of the metal. ΔT describes the temperature difference between its initial temperature T_0 and the melting temperature T_{melt}. $A(\lambda, T)$ is the wavelength and temperature dependent absorption coefficient of electromagnetic radiation for the material. J_{max} is a constant for which a value of 0.52 can be assumed for small focal point diameters and low scan speeds of the radiation source [21]. For the scenario described in this article, $I_{th_{min}}$ was calculated with a value of 3403 K for ΔT and an absorption coefficient of 0.42 [2]. The calculated minimum required intensity $I_{th_{min}}$ to melt tungsten is according to equation (2) with the given setup roughly 1.25 kW mm^{-2}. Assuming a laser beam with a focal point diameter of 2 mm gives 3.9 kW of power, matching very well with the experimentally determined lower limit of 4 kW (see Table 1). Moving with a scanning velocity of 800 mm min^{-1} the laser spends 0.15 s on an irradiated spot. Multiplied by the intensity $I_{th_{min}}$, this results in a required energy per unit area of roughly 187 J mm^{-2} in order to laser weld tungsten. Preliminary tests confirmed that tungsten could successfully be deposited on tungsten substrate by LMD-w with an energy per unit area of 191 J mm^{-2}.

Table 1 lists the process parameter range used for single welding

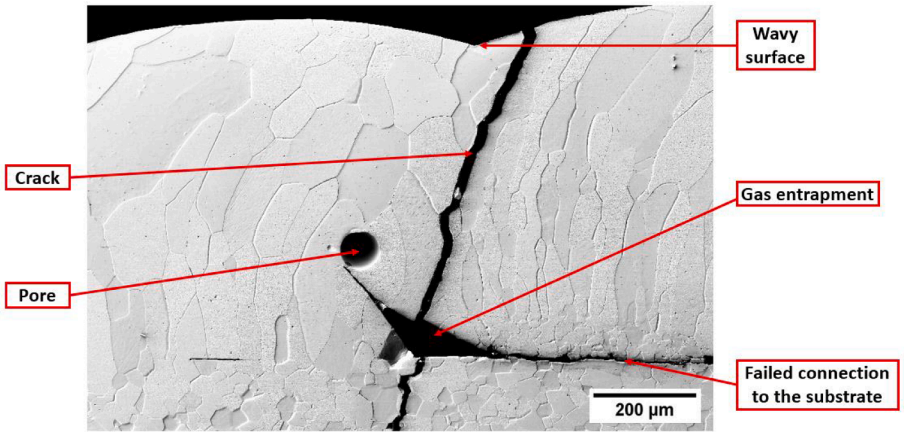

Fig. 3. SEM picture with an etched cross section of an LMD-w layer sample produced with 210 J mm^{-2}. Various defect types are highlighted.

beads. In context of this study, 45 individual beads were generated in order to gain an overview of the behaviour of tungsten for the LMD-w process. 9 of these beads are displayed in Fig. 2 (B).

In order to get closer to repairing damaged PFCs, the next step was the development and optimization of the generation of full layers. To build a layer, several welding beads are arranged at a certain distance (i.e., hatch distance) relative to each other. The parameter ranges investigated for layers are also listed in Table 1. Furthermore, the creation of stacked layers was tested and investigated. The layers were positioned on top of each other with the deposition direction rotated by 90° to ensure a uniform distribution of the material.

After the successful deposition of the material, some layers were melted a second time by the laser to test the influence of remelting on LMD-w produced layers. These experiments were carried out with the intent of minimizing the surface waviness and removing gas inclusions. During the remelting the working direction of the machine was rotated by 90° in comparison to the working direction during the layer creation to create a flat surface.

For the analysis, cross section views of polished/edged samples were prepared and examined by means of scanning electron microscopy (SEM; Zeiss LEO DSM 982 and Zeiss Cross Beam XB540) or light microscopy (Nikon Eclipse LV 100 D). The grain structure and orientation got investigated using electron backscatter diffraction (EBSD; Oxford instruments). Moreover, the resulting samples were analysed using a profilometer with a confocal sensor (KF3 by OPM GmbH).

3. Results and discussion

During the single-bead experiments, it became apparent that the seemingly random occurrence of balling defects first had to be eliminated. Fig. 2 (B) shows 9 of the welding beads that have been created. In this specimen, balling defects formed in the welding beads number 3 and 5. Close inspection revealed that the positioning of the tungsten wire in relation to the focal point of the laser has a strong influence on the formation of these balling defects. By precisely positioning the wire at the front edge of the melt pool created by the laser beam, the occurrence of balling defects was avoided completely in the subsequent LMD-w layer experiments. This positioning helps to ensure a sufficient performance in terms of surface finish, geometry control and defect free generation of the welding bead [23]. Through the single bead experiments the creation of individual welding beads has been optimized to such an extent that tungsten could be deposited reliably with minimal oxidation, good connection to the substrate and without balling defects. The surface of the tungsten deposited by LMD-w appears as a shiny metallic film, which is an indication of no or a very low level of impurities. The occurrence of tungsten oxides in the material deposited by LMD-w is unlikely because their boiling point is below the melting point of tungsten, which is the minimum reached temperature in the specified process. Furthermore, energy dispersive X-ray spectroscopy (EDX) measurements were carried out on material deposited by LMD-w and as a reference on the tungsten substrate material. These measurements showed that there is no difference in oxygen content between deposited material and the tungsten substrate material. The oxygen content in weight percent in each case is well below 1 %. There are no signs of tungsten carbides and other impurities in the deposited material, as these would be visible in the micrographs of the LMD-w layers but are not present in these and have not been detected by EDX.

However, new obstacles were encountered during the creation of tungsten LMD-w layers. Fig. 3 provides an overview of the various defect types which can occur during the generation of layers. The displayed layer was generated with an energy per unit area of 210 J mm^{-2}. Cracks can be observed in this etched cross section. The cut for this cross section was placed transversely to the deposition direction in the centre of the layer. The cracks have formed due to thermally induced peaks of residual stresses in the specimens. These residual stresses occur due to high temperature gradients between the molten tungsten and the cooled substrate plate during the solidification and cooling process.

Pores and gas entrapments, which are visible in Fig. 3, can have various origins. On the one hand, pores may remain in the solidified material because during the melting process gas can get trapped inside the material due to insufficient liquefaction or unfavourable flow transport. The flow dynamics in the melt pool are partially modeled by the dynamic viscosity (μ) described by the following equation [12,15,24,25]:

$$\mu = \frac{16\gamma}{15}\sqrt{\frac{m}{k_b T}}\left[kg\ m^{-1}s^{-1}\right] \tag{3}$$

where γ is the surface tension of the melt pool, m is the atomic mass, k_b is the Boltzmann-constant, and T the temperature in the melt pool. For tungsten, a surface tension of $\gamma = 2.48\text{–}0.31 \times 10^{-3}\ (T - T_m)$ can be assumed [26,27]. It can be seen that an increase of the temperature reduces the surface tension and also decreases the dynamic viscosity and thus minimizes the occurrence of associated defects like gas entrapments. Lowering the surface tension also improves the ability of the deposited liquid metal to wet and to connect to the substrate. This way, the occurrence of insufficient connection to the substrate defects can be reduced by increasing the energy. On the other hand, too high energy input during laser-based AM processes should be avoided because the probability of so-called keyhole defects increases. Keyhole defects are spherical pores that originate from the gas void that forms in the melt pool at the striking point of the laser [28]. The area density was determined from a contrast analysis of the micrographs at the first and at the last development stage using the image analysis program ImageJ. This density was increased from 94.8 % to 97.5 % by increasing the energy

Table 2
The surface waviness increases slightly with growing number of stacked layers and can be significantly reduced by remelting.

Experiment	Symbol	1 Layer	2 Layers stacked	3 Layers stacked	4 Layers stacked	1 Layer remelted (A)	1 Layer remelted (B)	Unit
Energy per unit area	E_n	477	477	477	477	477	955	J mm^{-2}
Initial position on the z-axis	d_v	0	+0.65	+1	+1.5	+0.65	+0.65	mm
Surface waviness	W_t	159	226	244	238	128	95	µm

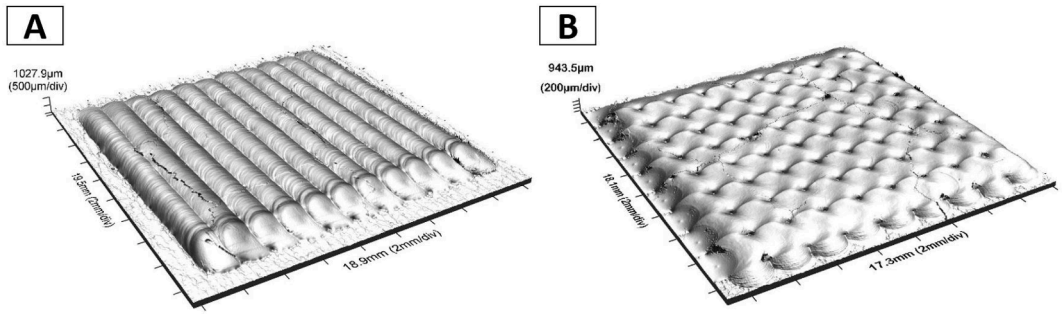

Fig. 5. These measurements of surface topologies were generated by laser profilometry. Tungsten layers were generated and remelted with an energy per unit area of 477 J mm^{-2}. (A) showing a normal layer and (B) showing a remelted layer. For remelting the scan direction was rotated by 90 degrees in order to decrease the surface waviness.

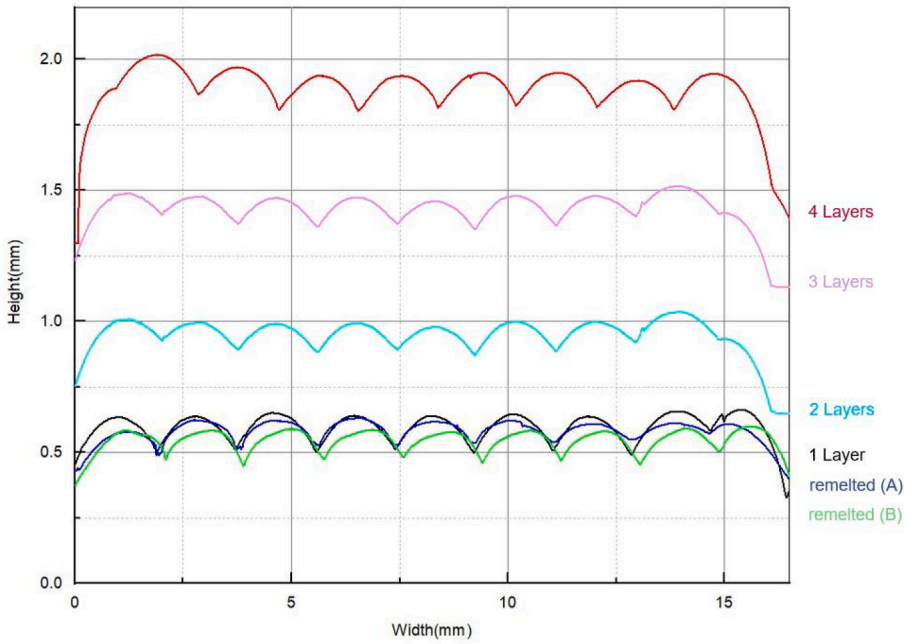

Fig. 4. Line profiles of various LMD-w layers which were measured by laser profilometry. These layers were deposited with the process parameters specified in Table 3. In the case of the remelted layer (A) and (B) an energy per unit area of 477 J mm^{-2} and 955 J mm^{-2} (halving the velocity), respectively was used.

per unit area and the hatch (distance between the welding beads), which led to a reduction in the defect density.

In the latest parametric studies for layers, the temperature in the melt pool was elevated by increasing the energy per unit area. Thereby the maximum power of the laser of 5 kW and the lowest tolerable deposition velocity was used. For all specimens discussed in Table 2 a deposition velocity of 400 mm min^{-1} was applied. Only for the "1 Layer remelted (B)" specimen a lower deposition velocity of 200 mm min^{-1} was applied to increase the energy input even further. These experiments were carried out with a hatch distance h_d of 1.51 mm and a deposition/scanning length L 14 mm. The layers were generated with a wire fed velocity v_w of 500 mm min^{-1}. The energy per unit area and the initial position on the z axis used for these experiments, as well as the resulting surface waviness of the specimens that were measured by laser profilometry are listed in Table 2. The surface waviness value W_t of the respective profile is maximum distance between the highest peak and the deepest valley of the filtered evaluation length profile. For the experiments described in Table 2, the surface waviness W_t of single, stacked, and remelted layers were compared.

The surface waviness is higher for 2 stacked layers than for a single layer. However, the values of 3 and 4 stacked layers are almost equal to the value of 2 stacked layers, i.e., it seems to saturate at about 240 µm. Whether this is acceptable or not has to be investigated in the future, but it was successfully demonstrated that it can be reduced by remelting, for instance by comparing the W_t values in Table 2 or by comparing Fig. 5 (A) and (B). Due to remelting, the maximum layer height of roughly 650

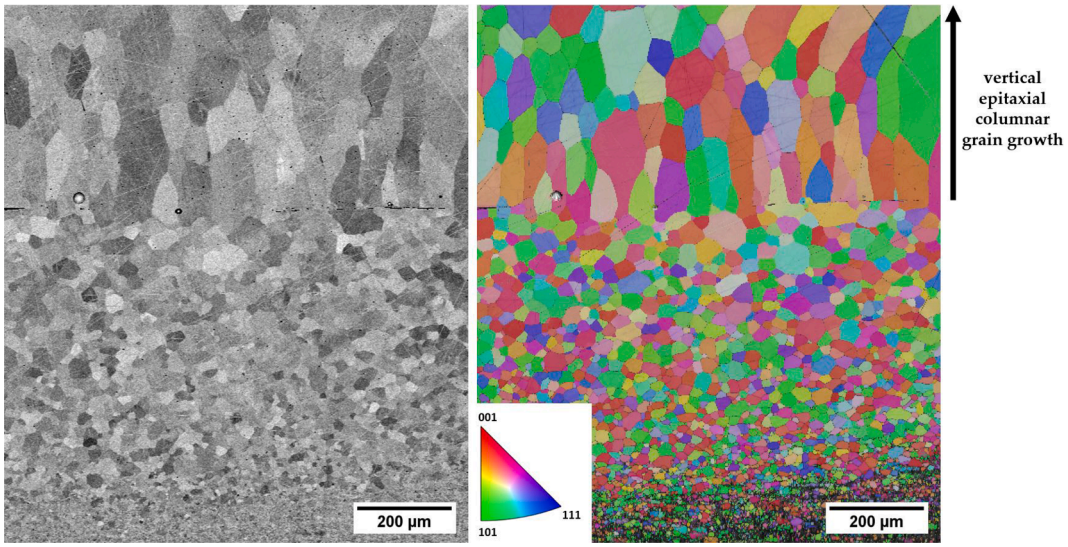

Fig. 6. SEM (left) and EBSD picture (right) with material deposited via LMD-w on top, the heat affected zone of the substrate material in the middle and the original, rolled substrate material at the bottom (the information is encoded in colors). This material was deposited with an energy per unit area of 210 J mm^{-2}.

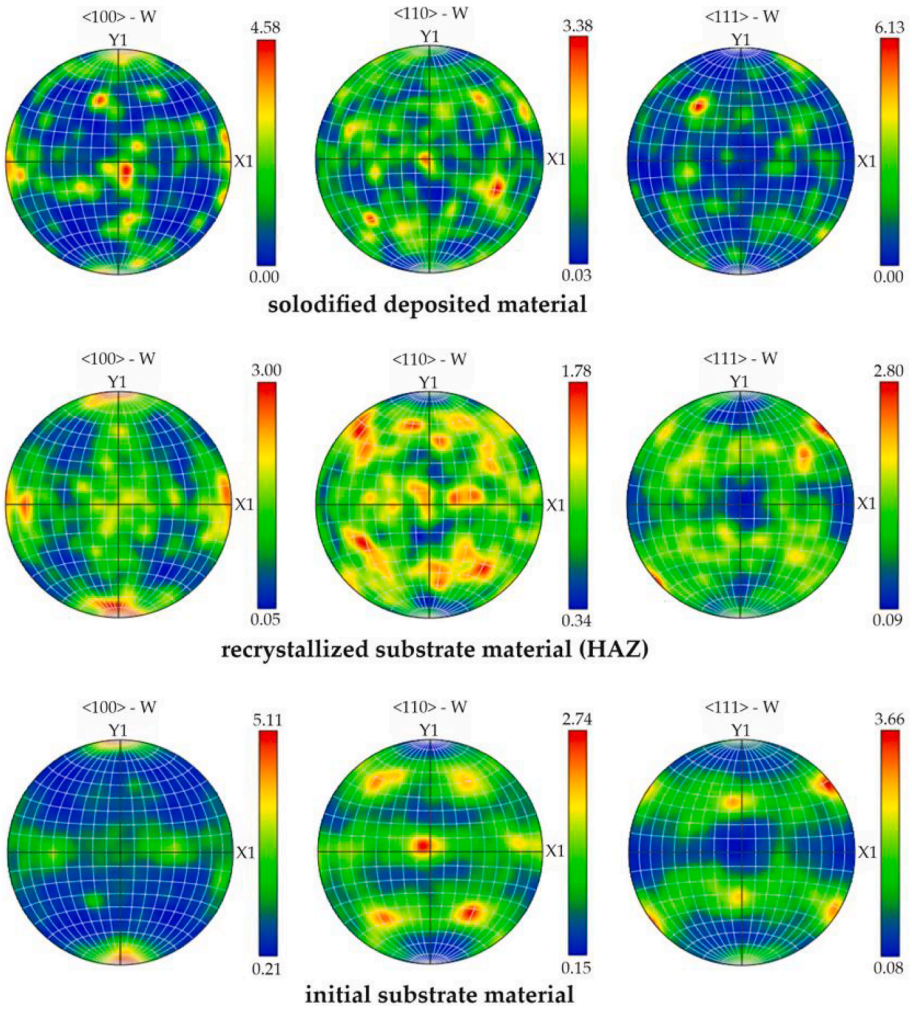

Fig. 7. Stereographic pole figures of (1 0 0), (1 1 0) and (1 1 1) for the solidified deposited material, the recrystallized material in the HAZ of the substrate and the initial rolled substrate material determined from the EBSD data (the information is encoded in colors).

Table 3
The most suitable parameters for the generation of tungsten layers on tungsten substrate using the LMD-w process under the specified conditions.

Process parameter	Symbol	Value	Unit
Energy per unit area	E_d	477	J mm^{-2}
Laser power	P	5	kW
Deposition velocity	v_t	400	mm min^{-1}
Wire fed velocity	v_w	500	mm min^{-1}

μm got decreased by about 50 μm. The maximum height of 2, 3 and 4 stacked layers measures roughly 1 mm, 1.5 mm, and 2 mm, respectively (see Fig. 4).

Additive manufacturing of metallic products in combination with high deposition rates is usually characterized by high process temperatures and slow cooling rates. This can lead to rather large and highly oriented columnar grains, grown along the building direction [11,22]. This columnar grain structure can be recognized also in the tungsten deposited here by LMD-w, e.g., in the upper region of Fig. 6. The grains in the deposited material have epitaxially grown from the substrate and are elongated in the z-direction. These grains have solidified from the liquid phase and have an average area of 3240 μm^2 and an aspect ratio of 2.3. Due to the reduced risk of grain release by cracking, this elongated grain structure transversal to the surface is particularly suitable for use as PFM [29]. The recrystallized substrate material in the heat affected zone (HAZ), in contrast, has smaller grains with an average area of 500 μm^2 and an average aspect ratio of close to 1, thus a clear sign of recrystallization. The size of these recrystallized grains in the HAZ, which is about 640 μm thick, decreases with increasing depth. The original substrate material shown in the bottom of Fig. 6 has comparatively small grains with an average area of 73 μm^2, which are flat in the x–y plane due to rolling. These grains in the original substrate material have an aspect ratio of 3.1. The EBSD image in Fig. 6 and the stereographic pole figures in Fig. 7 show that the deposited and the recrystallized grains in the HAZ do not have a preferential crystal orientation, i.e. no texture. In contrast, the initial substrate shows a clear (1 1 0) orientation. In most layer-by-layer AM processes, nucleation of new grains starts in the underlying unmolten material if the layers have the same chemical composition [11,22,30–32]. In the regions where there is sufficient bonding between deposited and substrate material, this nucleation behavior is also evident.

4. Summary & conclusions

Recent developments in AM technology offer new application opportunities. Within this study, the possibility of surface regeneration of plasma facing tungsten components using the LMD-w process is explored. It has been proven that the deposition of tungsten on tungsten substrates using the LMD-w process is possible. First, the generation of single melt paths was optimized. Afterwards, the generation of whole layers and stacked layers was optimized. Finally, it was demonstrated that the surface waviness increases with growing number of stacked layers and can be reduced below 100 μm by remelting. The most suitable parameters for the generation of layers with the setup described are listed in Table 3. The microstructure of the solidified deposited material consists of large epitaxially grown grains elongated in the z-direction but with arbitrary crystal orientations. The grains in the HAZ are recrystallized and decrease in size with increasing depth from the surface.

The process parameter adjustments discussed in this study have minimized the probability of occurrence of many typical LMD-w defect types. In order to eliminate the remaining defects such as gas entrapment and cracks, a heated substrate plate and an evacuated or inert gas filled process chamber would be necessary. Other powder bed-based AM studies have shown that a substrate temperature of 1000 °C can effectively reduce crack density and porosity [9–11]. This high temperature is not only far above the brittle to ductile transition temperature but also reduces the temperature gradients which occur during the process and thus lowers the residual stresses in the material. In situ process regulation mechanisms like for instance the resistance measurement-controlled LMD-w process would provide more opportunities for process stabilization [33,34]. Also combining continuous wave laser irradiation to melt the material and pulsed wave laser irradiation to distribute the liquid could further stabilize the process and counteract gas entrapment by increased liquefaction [19]. Furthermore, the use of thinner wire would open the possibility of generating more filigree shapes. This is especially interesting with respect to the edges of the generated layers and the waviness of their surface.

Concluding, the results are highly promising and provide the proof-of-principle as the generation of tungsten layers on tungsten substrate in good quality and in dimensions of divertor monoblocks is possible. Many of the issues usually encountered in additive manufacturing of tungsten do not occur in LMD-w processing, e.g., low porosity layers and stacking of layers without delamination are possible. Prospectively, it remains to be investigated to what extent, the process will allow the healing of damaged substrate surfaces, as will be the case in fusion reactors after plasma operation. Additionally, it requires investigation of how deposited layers behave under fusion relevant thermal loads. High heat flux (HHF) experiments will be carried out to validate the mechanical integrity of tungsten LMD-w layers.

Funding

This work has been carried out within the framework of the EUROfusion Consortium funded by the European Union via the Euratom research and training program (grant agreement no. 101052200—EUROfusion). The views and opinions expressed are, however, those of the authors only and do not necessarily reflect those of the European Union or the European Commission. Neither the European Union nor the European Commission can be held responsible for them.

CRediT authorship contribution statement

Jannik Tweer: Conceptualization, Formal analysis, Investigation, Methodology, Writing – original draft. **Robin Day:** Resources, Writing – review & editing. **Thomas Derra:** Resources, Writing – review & editing. **Daniel Dorow-Gerspach:** Conceptualization, Supervision, Writing – review & editing. **Thorsten Loewenhoff:** Conceptualization, Writing – review & editing. **Marius Wirtz:** Conceptualization, Writing – review & editing. **Christian Linsmeier:** Project administration, Supervision. **Thomas Bergs:** Resources, Writing – review & editing. **Ghaleb Natour:** Supervision, Writing – review & editing.

Declaration of competing interest

The authors declare that they have no known competing financial interests or personal relationships that could have appeared to influence the work reported in this paper.

Data availability

Data will be made available on request.

Acknowledgment

The author would like to thank: The colleagues from the Fraunhofer Institute for Production Technology for offering the opportunity to work with their equipment at their facility and for the adaptation of their LMD-w process from steel to tungsten. Noah Richter and Beatrix Göths for assistance in the mechanical preparation of the samples. Gaby Esser for performing the profilometer scans and Marcin Rasinski for his work in context of the EBSD investigation.

References

[1] T.R. Barrett, G. Ellwood, G. Pérez, M. Kovari, M. Fursdon, F. Domptail, S. Kirk, S. C. McIntosh, S. Roberts, S. Zheng, L.V. Boccaccini, J.-H. You, C. Bachmann, J. Reiser, M. Rieth, E. Visca, G. Mazzone, F. Arbeiter, P.K. Domalapally, Progress in the engineering design and assessment of the European DEMO first wall and divertor plasma facing components, Fusion Eng. Des. 109-111 (2016) 917–924.

[2] E.S. Lassner, W.D. Schubert, Tungsten: Properties, Chemistry, Technology of the Element, Alloys, and Chemical Compound, 1st ed., 1999, doi: 10.1007/978-1-4615-4907-9.

[3] J. Linke, et al., Challenges for plasma-facing components in nuclear fusion, Matter Radiat. Extrem. 4 (5) (2019), https://doi.org/10.1063/1.5090100.

[4] M.Z. Tokar, An assessment for the erosion rate of DEMO first wall, Nucl. Fusion 58 (1) (2018) 016016.

[5] T.h. Loewenhoff, S. Antusch, G. Pintsuk, M. Rieth, M. Wirtz, High pulse number thermal shock testing of tungsten alloys produced by powder injection molding, Nucl. Mater. Energy 20 (2019) 100680, https://doi.org/10.1016/j.nme.2019.100680.

[6] M. Wirtz, J. Linke, T. Loewenhoff, G. Pintsuk, I. Uytdenhouwen, Transient heat load challenges for plasma-facing materials during long-term operation, Nucl. Mater. Energy 12 (2017) 148–155, https://doi.org/10.1016/j.nme.2016.12.024.

[7] A. Loarte, B. Lipschultz, A.S. Kukushkin, G.F. Matthews, P.C. Stangeby, N. Asakura, G.F. Counsell, G. Federici, A. Kallenbach, K. Krieger, A. Mahdavi, V. Philipps, D. Reiter, J. Roth, J. Strachan, D. Whyte, R. Doerner, T. Eich, W. Fundamenski, A. Herrmann, M. Fenstermacher, P. Ghendrih, M. Groth, A. Kirschner, S. Konoshima, B. LaBombard, P. Lang, A.W. Leonard, P. Monier-Garbet, R. Neu, H. Pacher, B. Pegourie, R.A. Pitts, S. Takamura, J. Terry, E. Tsitrone, T.-O. Group, Chapter 4: power and particle control, Nucl. Fusion 47 (6) (2007) S203–S263.

[8] V. Barabash, G. Federici, R. Matera, A.R. Raffray, I. H. Teams, Armour materials for the ITER plasma facing components, Phys. Scr. T81 (1) (1999) 74.

[9] A.v. Müller, D. Dorow-Gerspach, M. Balden, M. Binder, B. Buschmann, B. Curzadd, T. Loewenhoff, R. Neu, G. Schlick, J.H. You, Progress in additive manufacturing of pure tungsten for plasma-facing component applications, J. Nucl. Mater. 566 (2022) 153760.

[10] A.v. Müller, G. Schlick, R. Neu, C. Anstätt, T. Klimkait, J. Lee, B. Pascher, M. Schmitt, C. Seidel, Additive manufacturing of pure tungsten by means of selective laser beam melting with substrate preheating temperatures up to 1000 °C, Nucl. Mater. Energy 19 (2019) 184–188.

[11] D. Dorow-Gerspach, A. Kirchner, T.h. Loewenhoff, G. Pintsuk, T. Weißgärber, M. Wirtz, Additive manufacturing of high density pure tungsten by electron beam melting, Nucl. Mater. Energy 28 (2021) 101046.

[12] S.-H. Pan, G.-C. Yao, Y.-N. Cui, F.-S. Meng, C. Luo, T.-Q. Zheng, G. Singh, Additive manufacturing of tungsten, tungsten-based alloys, and tungsten matrix composites, Tungsten 5 (1) (2023) 1–31.

[13] V. Philipps, R. Neu, J. Rapp, U. Samm, M. Tokar, T. Tanabe, M. Rubel, Comparison of tokamak behaviour with tungsten and low-Z plasma facing materials, Plasma Phys. Control. Fusion 42 (12B) (2000) B293–B310.

[14] T. Bergs, S. Kammann, G. Fraga, J. Riepe, K. Arntz, Experimental investigations on the influence of temperature for Laser Metal Deposition with lateral Inconel 718 wire feeding, Proc. CIRP 94 (2020) 29–34, https://doi.org/10.1016/j.procir.2020.09.007.

[15] J. Xie, H. Lu, J. Lu, X. Song, S. Wu, J. Lei, Additive manufacturing of tungsten using directed energy deposition for potential nuclear fusion application, Surf. Coat. Technol. 409 (2021) 126884, https://doi.org/10.1016/j.surfcoat.2021.126884.

[16] W. Jeong, Y.-S. Kwon, D. Kim, Three-dimensional printing of tungsten structures by directed energy deposition, Mater. Manuf. Process. 34 (9) (2019) 986–992, https://doi.org/10.1080/10426914.2019.1594253.

[17] G. Marinelli, et al., Microstructure and thermal properties of unalloyed tungsten deposited by Wire+ Arc Additive Manufacture, J. Nucl. Mater. 522 (2019) 45–53, https://doi.org/10.1016/j.jnucmat.2019.04.049.

[18] G. Marinelli, F. Martina, S. Ganguly, S. Williams, Development of Wire + Arc additive manufacture for the production of large-scale unalloyed tungsten components, Int. J. Refract. Metals Hard Metals 82 (2019) 329–335, https://doi.org/10.1016/j.ijrmhm.2019.05.009.

[19] M. Gipperich, et al., Reflectometry-based investigation of temperature fields during dual-beam Laser Metal Deposition, in: Laser 3D Manufacturing VIII, 2021, https://doi.org/10.1117/12.2576112.

[20] M. Gipperich, J. Riepe, R. Day, T. Bergs, express wire coil cladding (EW2C) as an advanced technology to accelerate additive manufacturing and coating, in: ASME Turbo Expo 2021: Turbomachinery Technical Conference and Exposition, 2021, Vol. 7: Industrial and Cogeneration; Manufacturing Materials and Metallurgy, V007T17A001, doi: 10.1115/gt2021-58709.

[21] K.H. Leong, H.K. Geyer, K.R. Sabo, P.G. Sanders, Threshold laser beam irradiances for melting and welding, J. Laser Appl. 9 (5) (1997) 227–231, https://doi.org/10.2351/1.4745464.

[22] M. Froend, V. Ventzke, F. Dorn, N. Kashaev, B. Klusemann, J. Enz, Microstructure by design: an approach of grain refinement and isotropy improvement in multi-layer wire-based laser metal deposition, Mater. Sci. Eng. A 772 (2020) 138635, https://doi.org/10.1016/j.msea.2019.138635.

[23] W.U.H. Syed, L. Li, Effects of wire feeding direction and location in multiple layer diode laser direct metal deposition, Appl. Surf. Sci. 248 (1–4) (2005) 518–524, https://doi.org/10.1016/j.apsusc.2005.03.039.

[24] D.D. Gu, W. Meiners, K. Wissenbach, R. Poprawe, Laser additive manufacturing of metallic components: materials, processes and mechanisms, Int. Mater. Rev. 57 (3) (2013) 133–164, https://doi.org/10.1179/1743280411y.0000000014.

[25] C. Tan, K. Zhou, W. Ma, B. Attard, P. Zhang, T. Kuang, Selective laser melting of high-performance pure tungsten: parameter design, densification behavior and mechanical properties, Sci. Technol. Adv. Mater. 19 (1) (2018) 370–380, https://doi.org/10.1080/14686996.2018.1455154.

[26] P.-F. Paradis, T. Ishikawa, R. Fujii, S. Yoda, Physical properties of liquid and undercooled tungsten by levitation techniques, Appl. Phys. Lett. 86 (4) (2005) 041901.

[27] P. Tolias, Analytical expressions for thermophysical properties of solid and liquid tungsten relevant for fusion applications, Nucl. Mater. Energy 13 (2017) 42–57, https://doi.org/10.1016/j.nme.2017.08.002.

[28] J.V. Gordon, S.P. Narra, R.W. Cunningham, H.e. Liu, H. Chen, R.M. Suter, J. L. Beuth, A.D. Rollett, Defect structure process maps for laser powder bed fusion additive manufacturing, Addit. Manuf. 36 (2020) 101552, https://doi.org/10.1016/j.addma.2020.101552.

[29] M. Wirtz, J. Linke, T.h. Loewenhoff, G. Pintsuk, I. Uytdenhouwen, Thermal shock tests to qualify different tungsten grades as plasma facing material, Phys. Scr. T167 (2016) 014015, https://doi.org/10.1088/0031-8949/t167/1/014015.

[30] Y. Chen, F. Lu, K.e. Zhang, P. Nie, S.R. Elmi Hosseini, K. Feng, Z. Li, P.K. Chu, Investigation of dendritic growth and liquation cracking in laser melting deposited Inconel 718 at different laser input angles, Mater. Des. 105 (2016) 133–141.

[31] M.S.F. de Lima, S. Sankaré, Microstructure and mechanical behavior of laser additive manufactured AISI 316 stainless steel Stringers, Mater. Des. 55 (2014) 526–532, https://doi.org/10.1016/j.matdes.2013.10.016.

[32] T. DebRoy, H.L. Wei, J.S. Zuback, T. Mukherjee, J.W. Elmer, J.O. Milewski, A. M. Beese, A. Wilson-Heid, A. De, W. Zhang, Additive manufacturing of metallic components – process, structure and properties, Prog. Mater Sci. 92 (2018) 112–224.

[33] P. Hagqvist, A. Heralić, A.-K. Christiansson, B. Lennartson, Resistance measurements for control of laser metal wire deposition, Opt. Lasers Eng. 54 (2014) 62–67, https://doi.org/10.1016/j.optlaseng.2013.10.010.

[34] P. Hagqvist, A. Heralić, A.-K. Christiansson, B. Lennartson, Resistance based iterative learning control of additive manufacturing with wire, Mechatronics 31 (2015) 116–123, https://doi.org/10.1016/j.mechatronics.2015.03.008.